

Laser Measurement of Anomalous Electron Diffusion in a Crossed-Field Plasma

Parker J. Roberts^{*} and Benjamin A. Jorns[†]
University of Michigan, Ann Arbor, Michigan 48109, USA

 (Received 16 December 2023; revised 8 February 2024; accepted 1 March 2024; published 26 March 2024)

The anomalous diffusion of particles and energy in magnetized plasma systems is a widespread phenomenon that can adversely impact their operation and preclude predictive models. In this Letter, this diffusion is characterized noninvasively in a low-temperature, Hall-type plasma. Laser-induced fluorescence and incoherent Thomson scattering measurements are combined with a 1D generalized Ohm's law to infer the time-averaged inverse Hall parameter, a transport coefficient that governs cross-field diffusion. While the measured diffusion profile agrees with model-based estimates in magnitude, the measurements do not exhibit the steep “transport barrier” typically imposed in models. Instead, these results show that the electric field is primarily driven by a diamagnetic contribution due to the large peak electron temperature exceeding 75 eV. This finding motivates a reconsideration of nonclassical energy transport across field lines in low-temperature plasmas.

DOI: [10.1103/PhysRevLett.132.135301](https://doi.org/10.1103/PhysRevLett.132.135301)

Electron diffusion across confining magnetic fields is exhibited by nearly all types of magnetized plasma [1–5]. Classically, this cross-field migration results from collisions with heavier species. In practice, however, such collisions are often insufficient to explain the measured rates of cross-field electron flux [6–10]. This “anomalous” transport can be orders of magnitude higher than the classical prediction. Enhanced diffusion poses a particular challenge for the low-temperature, crossed-field plasma devices—such as Hall and Penning discharges—that are widely employed for commercial and research applications [11,12]. It has been shown that the high electron transport adversely impacts the efficiency and ion beam quality in these devices, while also curtailing the development of fully predictive models [13,14]. These practical considerations have motivated an extensive body of investigations into electron transport in such systems [14–19]. Despite these efforts, however, the process remains poorly understood.

One of the major impediments for advancing understanding of anomalous diffusion in low-temperature plasmas stems from the sparsity of experimental data. While global consequences of the transport are measurable, such as the fractional current carried by electrons in the far field [20], locally resolving electron diffusion has been largely intractable to date. Standard physical probing methods have historically proven to be ineffective in the near field, as they are too perturbative or cannot resolve the highly directional electron drift [21,22]; moreover, previous nonintrusive experimental techniques to estimate the diffusion require strong and potentially unphysical assumptions [23,24]. In light of these challenges, it has become common practice to use calibrated models to infer the diffusion. This can be done, for example, by treating the electron diffusion with an effective transport coefficient, e.g., an anomalous collision

frequency [25,26]. This parameter is then prescribed locally and used to solve the governing equations in a multifluid or hybrid model for the discharge. The transport coefficient is adjusted iteratively until model predictions agree with more tractable, nonintrusive measurements, such as the ion velocity. This approach has been applied extensively to magnetized plasmas [19,27–31]. However, this indirect approach has several limitations, including questions about the fidelity and uniqueness of the inferred transport profile [32,33]. In light of these challenges, there is a pressing need to noninvasively infer the electron diffusion in these types of poorly understood crossed-field plasmas.

In this Letter, we present direct measurements of the anomalous cross-field electron diffusion as quantified by an effective transport coefficient. We achieve this based on a combination of two laser velocimetry diagnostics. First, laser-induced fluorescence (LIF) is a widely used benchmark tool to characterize ion acceleration and the electric field strength in low-temperature plasmas [34,35]. Second, incoherent Thomson scattering (ITS) is a method to measure the electron velocity distribution that has only recently been extended to have sufficient sensitivity for the low-temperature, low-density plasma regime by the work of Vincent *et al.* [36,37]. We perform this experiment in one of the most common low-temperature, crossed-field plasma devices: a Hall effect accelerator. We then compare these measurements to a previously reported indirect estimate for anomalous transport from a calibrated model.

To motivate our approach, we show in Fig. 1 a schematic of a canonical, axisymmetric Hall accelerator. This device features an annular plasma channel subject to a radial magnetic field $\vec{B} = B_r \hat{r}$ crossed with an axial electric field $\vec{E} = E_z \hat{z}$. The magnetic field strength is tailored so that the

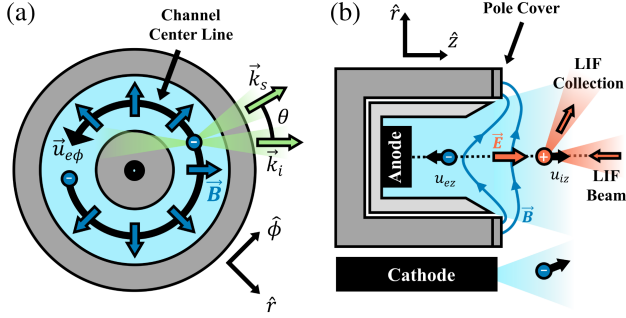


FIG. 1. Illustration of a Hall accelerator with the employed laser scattering geometry. (a) Front view with azimuthal Thomson scattering wave vectors. (b) Cross section of channel showing magnetic shielding geometry and axial laser-induced fluorescence injection scheme.

massive ions are effectively unmagnetized and accelerated by the electric field, while the electrons are magnetized. These electrons exhibit drifts described by a generalized Ohm's law,

$$u_{e\phi} = \frac{1}{\Omega^{-2} + 1} u_{\text{drift}}, \quad u_{ez} = -\frac{\Omega^{-1}}{\Omega^{-2} + 1} u_{\text{drift}}, \quad (1)$$

where $u_{\text{drift}} = E_z/B_r + [en_e B_r]^{-1} \partial_z(n_e k_B T_e)$ denotes the collisionless azimuthal drift arising from the electric field and diamagnetic effects, $-e$, n_e , and T_e are the electron charge, density, and temperature, and Ω is the Hall parameter representing the ratio of cyclotron frequency, $\omega_{ce} = eB_r/m_e$, to effective electron collision frequency (capturing both classical and nonclassical effects) [38]. Physically, the relations in Eq. (1) illustrate how the inverse Hall parameter, Ω^{-1} , can be interpreted as a transport coefficient. As Ω^{-1} increases, the azimuthal Hall drift decreases, while the cross-field drift is enhanced. We subsequently focus on experimentally characterizing this transport coefficient.

To this end, we consider three ways to relate the inverse Hall parameter to measurements of the background plasma properties based on Eq. (1):

$$\Omega_A^{-1} = \frac{-2u_{ez}/u_{\text{drift}}}{(1 + \sqrt{1 + 4u_{ez}/u_{\text{drift}}})},$$

$$\Omega_B^{-1} = -\frac{u_{ez}}{u_{e\phi}}, \quad \Omega_C^{-1} = \sqrt{\frac{u_{\text{drift}}}{u_{e\phi}}} - 1. \quad (2)$$

Method ‘‘C’’ is not feasible experimentally because the small value of $\Omega^{-1} \ll 1$ in strongly magnetized plasmas makes u_{drift} and $u_{e\phi}$ nearly indistinguishable; we thus only consider methods ‘‘A’’ and ‘‘B’’ in this work. Evaluating Ω^{-1} from these two formulas is possible given the electron density, temperature, axial velocity, and azimuthal velocity, in addition to the electric field.

We characterized these plasma properties on the discharge channel center line in the H9, a 9-kW-class Hall

effect accelerator [39]. We operated this device at a discharge voltage of 300 V and 15 A on krypton in the Alec D. Gallimore Large Vacuum Test Facility, at a pressure of 5 μTorr [40]. The H9 features a shielded magnetic topology, which protects the channel from plasma erosion [41,42]. This configuration leads to a downstream shift in the acceleration zone with larger electron temperatures compared to Hall devices without magnetic shielding [37,43].

To infer the electric field, E_z , we examined the axial ion velocity distribution function (IVDF) along the channel centerline. Following the method of Perez-Luna *et al.* [44], the statistical moments of this IVDF yielded estimates for the local electric field. We measured these distributions with the laser-induced fluorescence (LIF) system described in Ref. [45], which characterizes the Doppler-broadened line shape of a laser-induced transition from a metastable state of singly charged krypton ions. Non-Doppler broadening can be neglected for this regime such that the LIF line shapes approximate the IVDF along the laser wave vector [45,46]. Figure 1(b) illustrates the injected beam and collection optic, which intersected to form an interrogation point with 1-mm spatial resolution. This spot size was more than an order of magnitude smaller than the channel width. We moved this point in the axial direction relative to the Hall accelerator by translating the device on a motion stage, with $z = 0$ denoting the pole cover surface. Distances are normalized to the channel length, L_c , being the distance from the anode to the pole cover surface [cf. Fig. 1(b)]. Figures 2(a) and 2(b) show resulting IVDFs (with a velocity

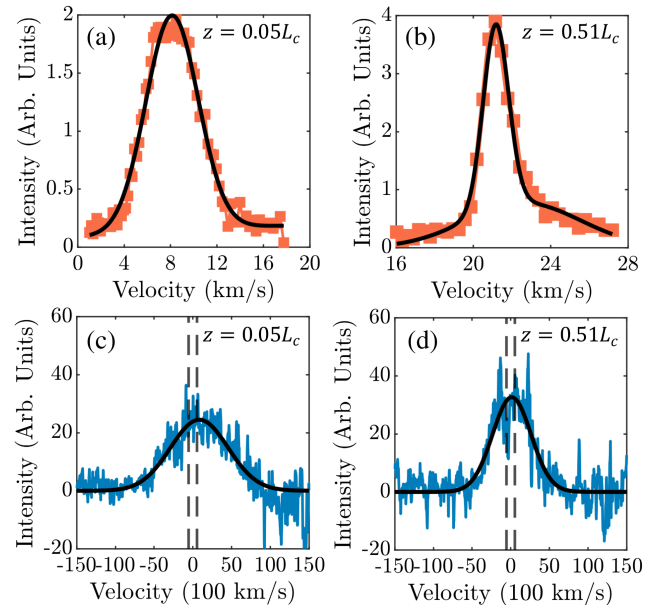


FIG. 2. (a),(b) Axial ion velocity distributions from laser-induced fluorescence with model fit, where L_c is the H9 channel length. (c),(d) Azimuthal electron velocity distributions from incoherent Thomson scattering with Maxwellian fit, showing notch filter stop band (dashed lines).

resolution of 200 m/s) at two locations along channel centerline, with fits to a sum of two Gaussian distributions (solid lines).

We used incoherent Thomson scattering (ITS) to directly measure the electron properties $u_{e\phi}$, n_e , and T_e along channel centerline. This diagnostic resolves the electron velocity distribution function (EVDF), inferred from the spectrum of light scattered by the plasma. As shown in Fig. 1(a), we focused a Q -switched Nd:YAG laser with wavelength $\lambda_0 = 532$ nm and a pulse energy of 700 mJ, into the plasma with wave vector \vec{k}_i . An *in situ* optic collected scattered radiation at wave vector \vec{k}_s , angled $\theta = 30^\circ$ from \vec{k}_i . An optical fiber routed this light to the detection bench described in Ref. [47], consisting of three volume Bragg grating stray light filters [36], a spectrometer, and an EMICCD camera. We averaged 3000 spectra at each location, subtracting the background emission. These plasma conditions and wavelength satisfied the incoherence condition [48], meaning that the power scattered at wavelength $\lambda = 2\pi/k_s$ is proportional to the number of electrons with velocity, v , projected along the scattering vector, $\Delta\vec{k} = \vec{k}_s - \vec{k}_i$. This proportionality is governed by a Doppler shift: $v(\lambda) = c(\lambda_0/\lambda - 1)/(2 \sin[\theta/2])$, where c is the speed of light, corresponding to a velocity resolution of 29 km/s. A motion stage provided spatial resolution, with $\Delta\vec{k}$ aligned to measure azimuthal velocities.

Figures 2(c) and 2(d) show azimuthal EVDFs at two locations. We extracted electron properties from these spectra by regressing a model for the convolution of a Maxwellian EVDF with the measured instrument broadening function $I(\lambda)$ [36,47]:

$$g(\lambda_k) = \sum_{\ell=1}^N \frac{H n_e r_e^2}{v_{Te} \sqrt{\pi}} e^{-\frac{(v(\lambda_\ell) - u_e)^2}{v_{Te}^2}} I(\lambda_k - \lambda_\ell), \quad (3)$$

where $v_{Te} = \sqrt{2k_B T_e / m_e}$ is the thermal velocity, r_e denotes the classical electron radius, and H is an intensity calibration factor we determined from Raman scattering on nitrogen. Figures 2(c) and 2(d) display fits of Eq. (3) to the ITS data outside of the notch filter bandwidth (dashed lines).

The prescription in Eq. (2) depends on the axial electron velocity, u_{ez} , while we measured only the azimuthal component. We estimated u_{ez} from the other plasma measurements by invoking current continuity, i.e., $u_{ez} = u_{iz} - J_z / (en_e)$, where J_z is the total axial current density on centerline. This formulation assumes symmetry about channel centerline and ignores radial ($\parallel B$) velocity gradients, which is justified by the high degree of beam collimation and electron force equilibration along field lines suggested by extensive experiments and models of Hall accelerators [41,42,49–52]. In order to estimate J_z , we used the conversion $\eta_b J_z = enu_{iz}|_{\text{end}}$, where η_b is the

device’s beam utilization efficiency and the subscript “end” denotes the furthest downstream measurement; this efficiency was determined to be $\eta = 0.83 \pm 0.04$ for this device and operating condition in previous work [53]. Physically, this efficiency value represents the fact that 80% of the plasma current is carried by ions according to a downstream probe. Our approximation also ignores the effects of Kr III ions, which carry $\sim 20\%$ of the ion current based on downstream plume measurements [54]. It can be shown from quasineutrality and current continuity that neglecting this population leads to an underestimation of u_{ez} by $< 7\%$, assuming that these ions are accelerated from the same starting potential as the Kr II ions targeted by our LIF scheme.

Armed with the LIF and ITS techniques, we show in Fig. 3 the time-averaged plasma properties along channel centerline. We display 95% credible intervals from the least-squares fit error. Figure 3(a) shows the ion velocity and electric field, demonstrating acceleration commensurate with the discharge voltage. The maximum electric field is located about 0.15 channel lengths upstream of the maximum magnetic field. We then show in Figs. 3(b) and 3(c) the electron azimuthal temperature, density, and axial velocity. The temperature and density exhibit maxima collocated with the electric field peak, while the axial electron velocity decreases near the magnetic field peak. This is consistent with the interpretation that the maximum magnetic field impedes the axial electron motion, requiring a larger electric field to support the discharge current. This electric field then ohmically heats electrons, while ion

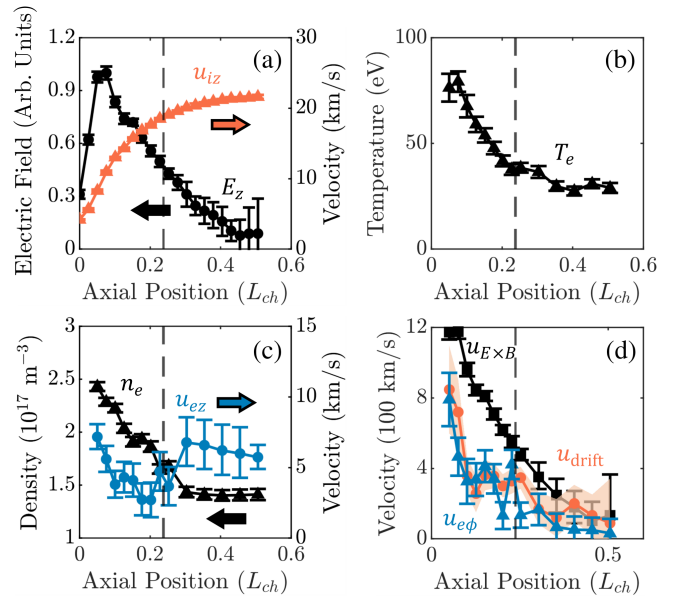


FIG. 3. Channel centerline plasma properties, with 95% credible intervals and magnetic field peak (dashed line). (a) Axial ion velocity and electric field. (b) Azimuthal electron temperature. (c) Electron density and axial electron velocity magnitude. (d) Azimuthal electron velocity compared to $u_{E \times B}$ and u_{drift} .

acceleration causes a decrease in the plasma density (cf. Ref. [13]).

Notably, the peak temperatures we measure, ~ 80 eV, are 2–2.5 times larger than measurements from both injected and wall-embedded probes [41], as well as predictions from models [29,55] of similarly configured ion sources. While similar electron temperatures have been measured in Hall accelerators with larger discharge voltages [56], previous probe measurements of shielded devices operating near 300 V have generally suggested T_e values close to 30–40 eV [41]. However, the magnitude of these measured temperatures is consistent with other Thomson scattering investigations of lower-power, magnetically shielded Hall accelerators [37]. This significant discrepancy with previous probe results may suggest that probe-based methods thermally perturb the plasma [21,22]. In turn, the contrast with modeling findings may indicate potential shortcomings in assumptions used to model electron energy transport [31,33], which we revisit in the following.

We show in Fig. 3(d) the directly measured azimuthal electron drift, $u_{e\phi}$. Overall, the drift is on the order of 100–800 km/s, approximately 10% of the electron thermal speed and 10–100 times higher than the axial drift. For comparison, we also show the $E \times B$ drift and the ideal, collisionless drift u_{drift} , which accounts for the diamagnetic drift. We estimate the latter by equating the axial temperature with the measured azimuthal temperature. The negative diamagnetic component reduces the value of the $E \times B$ drift by a factor of 2. While anisotropy is possible in the plasma, our use of azimuthal temperature is validated by the fact that the measured drift speeds agree with the collisionless values from the azimuthal temperature to within uncertainty. This agreement is also consistent with an inverse Hall parameter much smaller than unity [Eq. (1)], motivating *a posteriori* our decision to refrain from using method “C” for inferring the Hall parameter.

Having established the pertinent plasma measurements, we can now infer the inverse Hall parameter from both the computed collisionless drift value (method “A”) and from the directly measured azimuthal drift (method “B”). We show the resulting median estimates with 95% credible intervals propagated from the fit uncertainties in Fig. 4. We note here several features from these two methods. First, the credible intervals overlap over the domain, lending confidence to both methods and further addressing concerns about the use of azimuthal temperature in lieu of axial temperature in method “A.” Second, we note that at locations for which the credible intervals for u_ϕ and u_{drift} include zero, the inverse Hall parameter has no upper bound [cf. Fig. 3(d)]. In other words, the uncertainty in the inverse Hall parameter is large where the drift velocities are small. Third, we see that the median inverse Hall parameter estimates are nearly constant at $\Omega^{-1} \sim 0.01$ where E_z is large ($z < 0.2L_{ch}$), then increase to $\Omega^{-1} \sim 0.04\text{--}0.08$ at the downstream boundary. This relatively small upstream value

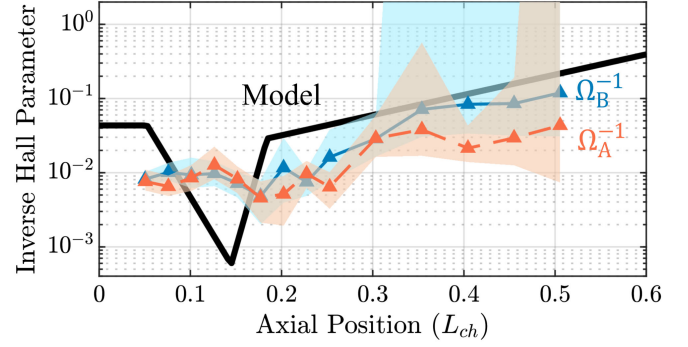


FIG. 4. Inverse Hall parameter measurements with 95% credible intervals from methods “A” and “B.” The solid line corresponds to the inverse Hall parameter calibrated for simulation results from Ref. [55].

is qualitatively consistent with previous experimental and numerical studies of these devices [15,24,29,33].

The results in Fig. 4 represent, to our knowledge, the most direct nonintrusive measurements of cross-field transport in this class of device performed to date. As such, these results represent a “ground truth” for evaluating model-based methods for inferring the inverse Hall parameter. To this end, we show for comparison in Fig. 4 values of the inverse Hall parameter determined from a model for this device and operating condition reported in previous work [45,55]. In that work, these values were tuned until a multifluid simulation matched LIF ion velocity data. The simulated and experimental results agree in overall magnitude. Moreover, all three profiles gradually increase in the region downstream of the peak magnetic field ($z/L_{ch} > 0.2$), which lends validation to the indirectly inferred profile.

Despite this agreement, there is a notable discrepancy that arises from this comparison: close to the peak in electric field, the simulation result differs from the nearly constant experimental values by an order of magnitude, instead exhibiting a sharp minimum. This minimum, which causes a localized barrier to cross-field transport, was thought to be necessary to capture the strong electric fields and match ion velocities from experimental measurement [29,33,57,58]. Our experiment suggests that in the real system, however, this transport barrier is not as stark as the simulation assumes, and is instead characterized by a wider, flatter transport curve.

Our results, then, invite the question as to how the system can physically support the measured electric fields in the absence of the strong transport barrier inferred from simulation. An explanation stems from another departure our results make from the simulation: the disparity between measured and simulated electron temperatures. As can be inferred from Eq. (1), in the limit of small inverse Hall parameter and for $u_{ez} < 0$, the electric field scales as $E_z = -\Omega B_r u_{ez} - (en_e)^{-1} \partial_z (n_e k_B T_e)$. In other words, for a fixed crossed-field drift, the electric field is moderated by the effective cross-field impedance, which scales with Ω .

There are consequently two ways to increase the electric field for a given cross-field drift: a lower inverse Hall parameter, or a stronger pressure gradient. Thus, although the inverse Hall parameter is larger than the simulated value, the plasma can still maintain the electric field by virtue of the higher experimentally observed temperatures.

With that said, the reason why models may underpredict the electron temperature by roughly a factor of 2 is an open question. Recent work suggests that this could arise from limitations in how models treat nonclassical energy diffusion [31]. It is a common practice, for example, to represent the anomalous heat flux with a Fourier law based on the same value of the inverse Hall parameter inferred for the electron drift [59,60]. Treating nonclassical heat transport with the same collision frequency used to describe momentum transport in this way is not well-supported—a fact that is demonstrated by the disagreement of our experimental temperature measurements with models. Additionally, these types of low-pressure plasmas ultimately rely on kinetic, rather than fluid, effects due to the long collisional mean free paths [61]. As a result, the energy balance may depend sensitively on nonlocal physics such as the secondary electron emission properties at the walls. Indeed, unshielded thrusters with low secondary electron emission wall materials have shown increased electron temperatures measured by injected probes [56].

As a concluding remark, we comment here on limitations of our methods. First, our measurements are time-averaged, whereas previous studies have suggested that Ω^{-1} fluctuates at frequencies of 10–100 kHz [46,62]. Our conclusions about the electron temperature and shallowness of the transport barrier may not apply equally to all phases of these fluctuations. Second, both our experiment and most fluid models do not account for effects of electron inertia, though some work suggests that these effects could play a non-negligible role in transport physics [63]. Even with these caveats, however, these findings represent new and direct insight into time-averaged particle diffusion across magnetic fields. The departures from our current understanding of this transport therefore invite a reconsideration of the assumptions used to model momentum and energy transport in low-temperature plasmas.

This work was supported by a NASA Space Technology Graduate Research Opportunity (Grant No. 80NSSC20K1229), the Air Force Office of Scientific Research Power and Propulsion Portfolio through a DURIP (FA9550-20-1-0191) and the Joint Advanced Propulsion Institute, a NASA Space Technology Research Institute. The authors would like to thank Dr. Zachariah Brown, Madison Allen, and William Hurley for experimental assistance, as well as Dr. Thomas Marks, Dr. Leanne Su, and Declan Brick for theoretical assistance.

*pjrob@umich.edu

†bjorns@umich.edu

- [1] D. Graham, Y. V. Khotyaintsev, M. André, A. Vaivads, A. Divin, J. Drake, C. Norgren, O. Le Contel, P.-A. Lindqvist, A. Rager *et al.*, *Nat. Commun.* **13**, 2954 (2022).
- [2] J. Taylor, *Phys. Rev. Lett.* **6**, 262 (1961).
- [3] D. Curreli and F. F. Chen, *Plasma Sources Sci. Technol.* **23**, 064001 (2014).
- [4] B. A. Carreras, *J. Nucl. Mater.* **337**, 315 (2005).
- [5] A. Bell, in *Laser Plasma Interactions 5* (CRC Press, Boca Raton, Florida, 2019), pp. 139–168.
- [6] P. B. Corkum, *Phys. Rev. Lett.* **31**, 809 (1973).
- [7] J. M. Urrutia and R. L. Stenzel, *Phys. Rev. Lett.* **57**, 715 (1986).
- [8] P. K. Shukla, *Phys. Rev. A* **36**, 4099 (1987).
- [9] M. Podestà, A. Fasoli, B. Labit, I. Furno, P. Ricci, F. M. Poli, A. Diallo, S. H. Müller, and C. Theiler, *Phys. Rev. Lett.* **101**, 045001 (2008).
- [10] K. Hara and S. Tsikata, *Phys. Rev. E* **102**, 023202 (2020).
- [11] J.-P. Boeuf, *J. Appl. Phys.* **121** (2017).
- [12] C. Phillips, *Proc. R. Soc. London* **64**, 172 (1899).
- [13] D. M. Goebel, I. Katz, and I. G. Mikellides, *Fundamentals of Electric Propulsion* (John Wiley & Sons, New York, 2023).
- [14] A. Anders, P. Ni, and A. Rauch, *J. Appl. Phys.* **111** (2012).
- [15] N. B. Meezan, W. A. Hargus, and M. A. Cappelli, *Phys. Rev. E* **63**, 026410 (2001).
- [16] N. B. Meezan and M. A. Cappelli, *Phys. Rev. E* **66**, 036401 (2002).
- [17] J. Carlsson, I. Kaganovich, A. Powis, Y. Raitses, I. Romadanov, and A. Smolyakov, *Phys. Plasmas* **25** (2018).
- [18] Z. A. Brown and B. A. Jorns, *Phys. Rev. Lett.* **130**, 115101 (2023).
- [19] A. Hecimovic, *J. Phys. D* **49**, 18LT01 (2016).
- [20] K. Dannenmayer and S. Mazouffre, *Plasma Sources Sci. Technol.* **22**, 035004 (2013).
- [21] B. Jorns, D. M. Goebel, and R. R. Hofer, in *Proceedings of the 51st AIAA/SAE/ASEE Joint Propulsion Conference* (American Institute of Aeronautics and Astronautics, Inc., Orlando, 2015), p. 4006.
- [22] L. Grimaud, A. Pétin, J. Vaudolon, and S. Mazouffre, *Rev. Sci. Instrum.* **87** (2016).
- [23] C. A. Thomas, N. Gascon, and M. A. Cappelli, *Phys. Rev. E* **74**, 056402 (2006).
- [24] E. T. Dale and B. A. Jorns, *Phys. Plasmas* **26**, 013516 (2019).
- [25] J. M. Fife, Hybrid-PIC modeling and electrostatic probe survey of Hall thrusters, Ph.D. thesis, Massachusetts Institute of Technology, 1998.
- [26] R. C. Davidson, *Plasma Phys.* **36**, 305 (1977).
- [27] W. Kruer and J. Dawson, *Phys. Fluids* **15**, 446 (1972).
- [28] E. Choueiri, *Phys. Plasmas* **6**, 2290 (1999).
- [29] I. G. Mikellides, B. Jorns, I. Katz, and A. Lopez Ortega, in *Proceedings of the 52nd AIAA/SAE/ASEE Joint Propulsion Conference* (2016), p. 4618.
- [30] K. Tummel, C. Ellison, W. Farmer, J. Hammer, J. Parker, and K. LeChien, *Phys. Plasmas* **27**, 092306 (2020).
- [31] T. A. Marks and B. A. Jorns, *J. Appl. Phys.* **134**, 153301 (2023).
- [32] I. G. Mikellides and A. L. Ortega, *Plasma Sources Sci. Technol.* **28**, 014003 (2019).

- [33] T. A. Marks and B. A. Jorns, *Plasma Sources Sci. Technol.* **32**, 045016 (2023).
- [34] G. Severn, X. Wang, E. Ko, and N. Hershkowitz, *Phys. Rev. Lett.* **90**, 145001 (2003).
- [35] R. Cedolin, W. Hargus Jr, P. Storm, R. Hanson, and M. Cappelli, *Appl. Phys. B* **65**, 459 (1997).
- [36] B. Vincent, S. Tsikata, S. Mazouffre, T. Minea, and J. Fils, *Plasma Sources Sci. Technol.* **27**, 055002 (2018).
- [37] B. Vincent, S. Tsikata, and S. Mazouffre, *Plasma Sources Sci. Technol.* **29**, 035015 (2020).
- [38] G. Hagelaar and N. Oudini, *Plasma Phys. Controlled Fusion* **53**, 124032 (2011).
- [39] R. R. Hofer, S. E. Cusson, R. B. Lobbia, and A. D. Gallimore, in *Proceedings of the 35th International Electric Propulsion Conference* (Electric Rocket Propulsion Society, 2017), pp. 2017–232.
- [40] E. A. Vigés, B. A. Jorns, A. D. Gallimore, and J. Sheehan, in *Proceedings of the 36th International Electric Propulsion Conference* (Electric Rocket Propulsion Society, Vienna, Austria, 2019), pp. 1–18.
- [41] R. R. Hofer, D. M. Goebel, I. G. Mikellides, and I. Katz, *J. Appl. Phys.* **115**, 043304 (2014).
- [42] I. G. Mikellides, I. Katz, R. R. Hofer, and D. M. Goebel, *J. Appl. Phys.* **115**, 043303 (2014).
- [43] S. E. Cusson, E. T. Dale, B. A. Jorns, and A. D. Gallimore, *Phys. Plasmas* **26**, 023506 (2019).
- [44] J. Pérez-Luna, G. Hagelaar, L. Garrigues, and J.-P. Boeuf, *Plasma Sources Sci. Technol.* **18**, 034008 (2009).
- [45] L. L. Su, T. A. Marks, and B. A. Jorns (to be published).
- [46] E. Dale, Investigation of the Hall thruster breathing mode, Ph.D. thesis, University of Michigan, 2019.
- [47] P. J. Roberts and B. Jorns, in *AIAA SCITECH 2023 Forum* (American Institute of Aeronautics and Astronautics, National Harbor, MD & Online, 2023).
- [48] J. Sheffield, D. Froula, S. H. Glenzer, and N. C. Luhmann Jr, *Plasma Scattering of Electromagnetic Radiation: Theory and Measurement Techniques* (Academic Press, New York, 2010).
- [49] L. Garrigues, G. Hagelaar, J. Bareilles, C. Boniface, and J. Boeuf, *Phys. Plasmas* **10**, 4886 (2003).
- [50] A. Morozov and V. Savelyev, *Rev. Plasma Phys.* **21**, 203 (2000).
- [51] W. Hargus, Jr and M. Cappelli, *Appl. Phys. B* **72**, 961 (2001).
- [52] X. Duan, M. Cheng, X. Yang, N. Guo, X. Li, M. Wang, and D. Guo, *J. Appl. Phys.* **127** (2020).
- [53] L. Su and B. Jorns, *J. Appl. Phys.* **130**, 160901 (2021).
- [54] L. L. Su, P. J. Roberts, T. Gill, W. Hurley, T. A. Marks, C. L. Sercel, M. Allen, C. B. Whittaker, M. Byrne, Z. Brown *et al.*, in *AIAA SCITECH 2023 Forum* (American Institute of Aeronautics and Astronautics, Inc., National Harbor, 2023), p. 0842.
- [55] L. L. Su, T. A. Marks, and B. A. Jorns, in *Proceedings of the 37th International Electric Propulsion Conference* (Electric Rocket Propulsion Society, Boston, MA, 2022).
- [56] Y. Raitses, I. D. Kaganovich, A. Khrabrov, D. Sydorenko, N. J. Fisch, and A. Smolyakov, *IEEE Trans. Plasma Sci.* **39**, 995 (2011).
- [57] T. Lafleur, S. Baalrud, and P. Chabert, *Phys. Plasmas* **23**, 053502 (2016).
- [58] T. Lafleur, S. Baalrud, and P. Chabert, *Phys. Plasmas* **23**, 053503 (2016).
- [59] I. G. Mikellides and I. Katz, *Phys. Rev. E* **86**, 046703 (2012).
- [60] O. Chapurin, A. Smolyakov, G. Hagelaar, J.-P. Boeuf, and Y. Raitses, *J. Appl. Phys.* **132** (2022).
- [61] I. D. Kaganovich, V. I. Demidov, S. F. Adams, and Y. Raitses, *Plasma Phys. Controlled Fusion* **51**, 124003 (2009).
- [62] T. Charoy, T. Lafleur, A. A. Laguna, A. Bourdon, and P. Chabert, *Plasma Sources Sci. Technol.* **30**, 065017 (2021).
- [63] R. Sahu, A. R. Mansour, and K. Hara, *Phys. Plasmas* **27** (2020).